Examining Lacunarity Approaches in Comparison with Fractal and Spatial Autocorrelation Techniques for Urban Mapping

Soe W. Myint and Nina Lam

Abstract

The conventional spectral-based classification techniques have often been criticized due to the lack of consideration of images' spatial properties. This study evaluates and compares two lacunarity methods, fractal triangular prism, spatial autocorrelation, and original spectral band approaches in classifying urban images. Results from this study show that the traditional spectral-based classification approach is inappropriate in classifying urban categories from high-resolution data. The fractal triangular prism approach was also found to be ineffective in classifying urban features. Spatial autocorrelation was more accurate than the fractal approach. The overall accuracies in this study for the fractal, conventional spectral, spatial autocorrelation, lacunarity binary, and lacunarity gray-scale approaches were 52 percent, 55 percent, 78 percent, 81 percent, and 92 percent, respectively. These findings suggest that the lacunarity approaches are far more effective than the other approaches tested and can be used to drastically improve urban classification accuracy.

Introduction

When extracting urban/suburban information from remotely sensed data, high spatial resolution images are needed to accurately distinguish the various urban features. The higher the spatial resolution of remotely sensed data, the higher the level of detailed objects and features in urban areas (e.g., single-family versus multi-family houses, roads, trees, grass, and parking lots) become apparent; therefore, the spectral response of an urban environment as a whole becomes more complex. When dealing with high-resolution remotely sensed data for urban land use and land cover mapping, the traditional spectral-based image classification techniques (sometimes referred to as per-pixel classifiers) have proven inadequate due to the lack of consideration of images' spatial properties (Green et al., 1993; Muller, 1997; Kiema and Bahr, 2001; Myint, et al., 2002; Myint, 2003a). This is because urban features are composed of spectrally different diverse materials (Jensen and Cowen, 1999) concentrated in a small area (e.g., plastic, metal, rubber, glass, cement, and wood). Hence, many objects and land cover features may need to be considered together and identified as one land use class (e.g., residential).

The high-frequency spatial appearance or complex nature of urban features is a major limitation in accurate urban land-use and land-cover classification using high-resolution image data (Myint et al., 2003; Myint, 2003b). Within-class variance and class boundary pixels are the two important issues that control the classification accuracy of images (Metzger and Muller, 1996). Traditional image processing algorithms (e.g., maximum likelihood classifier) do not take the local structure or the spatial arrangement of neighborhood pixels into consideration. This spatial information needs to be extracted, in addition to its individual spectral value, to characterize the heterogeneous nature of urban features in high-resolution images.

Another critical limitation for conventional supervised classification is that it is extremely difficult to define suitable training samples for many categories within urban environments. This is due to variation in the spectral response of their component land-cover types (Foster, 1985; Gong and Howarth, 1990; Barnsley et al., 1991; Myint, et al., 2002). Thus, the training statistics may exhibit very high standard deviation (Sadler et al., 1991) and violate one of the basic assumptions of the widely used maximum-likelihood decision rule, namely, that the pixel values follow a multivariate normal distribution (Barnsley et al., 1991; Sadler et al., 1991). Hence, there is an emerging need for an effective approach to accurately classify urban land-use and land-cover features using high-resolution image data.

There have been some attempts to improve the spectral analysis of remotely sensed data by using texture transforms, in which some measures of variability in DN values are estimated within local windows: e.g., contrast between neighboring pixels (Edwards et al., 1988), standard deviation (Arai, 1993), local variance (Ferro and Warner, 2002), Getis statistics (Wulder and Boots, 1998), or gray level co-occurrence matrix (GLCM) (Haralick et al., 1973; Franklin et al., 2000; Pesaresi, 2000). De Jong and Burrough (1995) analyzed variograms of remotely sensed images to quantitatively describe their spatial patterns. Variogram interpretation of satellite data was also carried out by Woodcock et al. (1988), Brown (1998), and Walsh et al. (2004).

Crews-Meyer (2002) used spatially nested pattern metrics (i.e., double-log fractal, interspersion index, percentage landscape area, and mean patch fractal dimension) to characterize landscape dynamism. Emerson et al. (1999)

Soe W. Myint is with the Department of Geography, 100 East Boyd Street, University of Oklahoma, Norman, OK 73019 (swmyint@ou.edu).

Nina Lam is with the Department of Geography, 227 Howe/ Russell Geoscience Complex, Louisiana State University, Baton Rouge, LA 70803 (nlam@lsu.edu).

analyzed the fractal dimension and the spatial autocorrelation of satellite imagery (using the isarithm method and Moran's *I* and Geary's *C*, respectively) to observe the differing spatial structures of the smooth and rough surfaces in remotely sensed images. Lam and Quattrochi (1992) demonstrated that the fractal dimension of remote sensing data could yield quantitative insight on the spatial complexity and information content contained within these data. Bian and Walsh (1993) and Walsh *et al*. (1997) used fractal analysis for assessing the effects of scale on landscape analysis. Quattrochi *et al*. (1997) developed a software package known as the Image Characterization and Modeling Systems (ICAMS) to examine how fractal dimension is related to surface texture. They also investigated how spatial resolution affects the computed fractal dimension of ideal fractal sets by using the isarithm, variogram, and triangular prism methods (Lam and De Cola, 1993; Mark and Aronson, 1984; Clarke, 1986; Lam *et al*., 2002).

Fractal dimensions may be viewed as a measure of irregularity or heterogeneity of spatial arrangements and physical processes in many fields of studies. There has been growing interest in the application of fractal geometry to characterize spatial complexity of geographic phenomena at multiple scales. The study of the relationship between physical processes and the effects of scale has become increasingly important in geographic information sciences. Mandelbrot (1983) defined the term fractal as "a set for which the Hausdorff Besicovitch dimension strictly exceeds the topological dimension." Fractal exemplifies the idea of self-similarity, in which the spatial behavior of a system, an object, or a group of features is independent of scale (Burrough, 1993; Turcotte, 1997). An ideal fractal curve or surface has a constant dimension value over all scales. The variability of many natural phenomena is often irregular, and sometimes it can be approximated by fractional Brownian motion (Mandelbrot, 1983).

Some researchers suggested that local fractal analysis of remotely sensed images may reveal information on different land-use and land-cover categories better than spectral-based classifier. A potential use of fractal dimension could be the analysis of texture information in image classification. Studies of image analysis and texture classification have been conducted by scholars in different disciplines over the past several decades with the expectation that different land-use and land-cover classes could be characterized by the fractal dimension values (Jaggi *et al*., 1993; de Jong and Burrough, 1995; Lam *et al*., 1998; Emerson *et al*., 1999; Kaplan, 1999; Qiu *et al*., 1999). While these analyses demonstrate the potential of fractal geometry in characterizing texture features in remotely sensed images, some researchers (e.g., Klinkenberg and Goodchild, 1992; Burrough, 1993; Roach and Fung, 1994; De Jong and Burrough, 1995; Dong, 2000) argue that fractal analyses of constructed sets do not provide a complete description of natural scaling phenomena, and remotely sensed images of land-cover units are not true fractals.

Mandelbrot (1995) reported that fractal dimensions may be far from providing a complete characterization of a set's texture. In other words, different fractal sets may share the same fractal dimension values and have different appearances or textures (Mandelbrot, 1983; Voss, 1986; Dong, 2000), just as different texture appearances of classes may share the same variance or mean value. As an initial step toward quantifying the texture or spatial arrangements of features, Mandelbrot (1983) introduced the term *lacunarity* (lacunar is Latin for "gap") to characterize different texture appearances, which may have the same fractal dimension value. Different fractal sets that have the same dimension value may be constructed, but they look completely different because they may have different lacunarities.

Lacunarity represents the distribution of gap sizes: low lacunarity geometric objects are homogeneous because all gap sizes are the same, whereas high lacunarity objects are heterogeneous (Dong, 2000). It is understood that objects that are homogeneous at a small scale can be heterogeneous at a larger scale. Therefore, lacunarity is a scale-dependent measure of spatial complexity or texture of a landscape (Plotnick *et al*., 1993). Unlike most other landscape indices and measures (Haines-Young and Chopping, 1996; Gustafson, 1998), the computed values of lacunarity are sensitive not to map boundaries, but to scale. It measures the deviation of a geometric structure from translational invariance, or gappiness of a geometric structure (Gefen *et al*., 1983). In this study, lacunarity, a new method for texture analysis, which can be expected to describe the characteristic of fractals of the same dimension with different texture appearances, was examined and evaluated in comparison with the fractal triangular prism, spatial autocorrelation, and traditional original spectral band approaches.

Data and Study Area

Multispectral Ikonos image data with 4 m spatial resolution with 4 channels: blue (0.45–0.52 μm), green (0.52–0.60 μm), red (0.63–0.69 μm), and near infrared (0.76–0.90 μm) was used for identifying urban land-use and land-cover categories. The image data was acquired over Norman, Oklahoma on 20 March 2000. A subset of Ikonos data (1102 pixels by 793 pixels), which contains the central part of the Norman metropolitan area, is shown in Figure 1. Instead of converting to 8-bit, the original 16-bit data was used, because we anticipated that higher radiometric resolution would help us better identify texture features using lacunarity approaches. Norman, Oklahoma offers an ideal site to examine the effectiveness of lacunarity approaches in identifying complex forms of land use classes. Norman is a small- to medium-sized city with a population of about 94,000. It represents a typical American city having common urban/suburban land-use and land-cover classes such as commercial, industrial, parks, agriculture, residential, schools, trees, shrubs, grass, and water categories. One other reason for selecting Norman as the study area was that the city does not have high-rise buildings (only 2 or 3 buildings with 10 to 15 stories). We believe that we may need to consider lidar data for accurate

Figure 1. A subset of Norman, Oklahoma metropolitan area, displayed using band 3 (0.63 μm to 0.69 μm).

mapping when dealing with mega cities with many high-rise buildings.

Examining the relationships between urban land-use, land-cover classes associated with surface vegetation, water availability, and associated temperature fluctuation within an urban area is crucial for city planners and environmental officers. This information will be useful for developing a better infrastructure management plan to avoid environmental degradation: air pollution, noise pollution, traffic congestion, urban heat island effect, chemical contamination, and soil loss due to improper urban development. We considered residential areas with different tree crown closure percents as very important categories for urban planning. Vegetation influences urban environmental conditions and energy fluxes (Gallo *et al.*, 1993; Owen *et al.*, 1998). The presence and abundance of vegetation in urban areas has long been recognized as a strong influence on energy demand and development of the urban heat island (Oke, 1982; Huang *et al.*, 1987). Urban vegetation abundance may also influence air quality and human health (Wagrowski and Hites, 1997). They also provide surface area for sequestration of particulate matter and ozone. The loss of trees in urban areas intensifies the urban heat island effect due to the loss of shade and evaporation and the loss of the principal absorbers of carbon dioxide and trappers of other pollutants.

Following Lo *et al.* (1997), seven urban land-use and land-cover features with different textural appearances were selected: residential areas with less than 50 percent tree canopy (Residential-1: R1), residential areas with more than 50 percent tree canopy (Residential-2: R2), commercial (C), woodland (F), agriculture (A), grassland (G), and water body (W). Although these land-use land-cover classes may not cover all classes in all cities, they are important for environmental planning and hence were selected for this study. Channels 4 (near infrared), 3 (red), and 2 (green) were used as the original multispectral bands in this study.

Residential land uses range from high density, defined as multiple dwelling units per acre, to low density, where houses are on lots of more than an acre (usually less than two units per acre), on the periphery of urban expansion. It should be noted that in our study area, the density of residential areas in the city is somewhat uniform, since Norman is a small- to medium-sized city with population less than 94,000. However, greenness, vegetation biomass content, or crown closure percent in different residential areas were found to be different. The residential strips generally have a uniform size and spacing of structures, linear driveways, linear sidewalks, trees, grass, shrubs, parking lots, swimming pools, cement roads, and tar roads. The rest of the classes were adopted using hybrid levels II and III categories of the USGS land use/land cover classification scheme (Anderson *et al.*, 1976) and modified by Florida Bureau of Comprehensive Planning (1976) (Sabins, 1997).

Methods

Lacunarity Approaches

A number of algorithms for computing lacunarity have been developed (Lin and Yang, 1986; Voss, 1986; Allain and Cloitre, 1991; Dong, 2000) after Mandelbrot (1983) introduced some computations for lacunarity in general form. Allain and Cloitre (1991) initiated a conceptually straightforward and computationally simple "gliding box" algorithm for calculating lacunarity, and reported that lacunarity appears to be a new tool for identifying the geometry of deterministic and random sets. Since lacunarity measures the heterogeneity or degree of complex spatial arrangement, a higher index value of lacunarity indicates a more heterogeneous feature, and vice versa.

Plotnick, *et al.* (1996) emphasized the concept and utilization of lacunarity for the characterization of spatial features, which may not be fractals. The gliding box algorithm has been used for calculating the lacunarity value of binary images, as well as gray-scale images. This study evaluates both the binary and the gray-scale methods for computing lacunarity and their accuracy in classifying urban features. We reported previously in Myint and Lam (2004), the development of lacunarity algorithms and initial exploration of lacunarity approaches. This study examined lacunarity in comparison with fractal and spatial autocorrelation approaches. Details of the computation of the two lacunarity approaches can be found in Myint and Lam (2004), with a brief overview of the two algorithms described as follows.

Lacunarity – Binary Approach

The gliding box of a specific size r (length of a square box) is first placed at the top left corner of an image in which each and every pixel is filled with either 1 or 0 (Allain and Cloitre, 1991; Plotnick, *et al.*, 1993). The term *gliding box*, as usually referred in the lacunarity literature, is comparable to moving window in filtering approaches. First, binary images were generated by converting each gray-scale image (each band) into four quartile images with value 1's and 0's. The image was basically sliced into five levels in order to get the four quartile images. The location of each quartile can be computed using the following formula:

$$\begin{cases} ((x_{(j)} + x_{(j+1)})/2 & if \quad g = 0 \\ x_{(j+1)} & if \quad g > 0 \end{cases} \quad (1)$$

where $n \times p = j + g$, j = quartile level and is an integer, g is the decimal portion, n = number of observations, p = cumulative frequency, e.g., for a data set of 8, to find Q_3, p is 0.75, and g becomes 0 ($8 \times 0.75 = 6 + 0$). Equation 1 is a common formula for finding percentiles and was used in this study to compute the quartile locations for the image. It is understood that minor variations of the above formula have been used, which could yield minor differences in quartile locations (Journet, 1999).

Then, the box mass "S," that is the number of occupied pixels (1's), is computed. The gliding box is systematically moved through the binary image one pixel at a time, and the box mass value is determined for each of the overlapping boxes. For a given box size r, the probability of box mass S is:

$$P(S, r) = \frac{n(S, r)}{N(r)} \quad (2)$$

where $n(S, r)$ is the number of gliding boxes of size r with mass S, and $N(r)$ is the total number of boxes of size r. The first and second moment of this distribution, $E(S)$ and $E(S^2)$ are:

$$E(S) = \sum SP(S, r), \text{ and} \quad (3)$$

$$E(S^2) = \sum S^2 P(S, r). \quad (4)$$

Lacunarity for gliding box size r, $\Lambda(r)$, is defined as:

$$\Lambda(r) = \frac{E(S^2)}{E^2(S)}. \quad (5)$$

Based on a random binary image which has only two values − 0 for empty and 1 for filled, it can be described as

$$E(S^2) = \text{var}(S) + E^2(S). \quad (6)$$

Plotnick *et al.* (1993) extended Equation 5 into

$$\Lambda(r) = \frac{\text{var}(S)}{E^2(S)} + 1 \quad (7)$$

where $E(S)$ is the mean, and var(S) is the variance of the number of occupied pixels per box.

We previously created six hypothetical 15 × 15 binary image patterns, with white pixels representing 1's and black pixels representing 0's, and demonstrated the measurement of these patterns using different gliding box sizes: r = 3, 5, 7, 9, and 11 using the binary approach. It was found that finer scales or smaller gliding box sizes (e.g., 3 × 3) provided notably different lacunarity values for different patterns. Hence, it is important to note that lacunarity can be used to measure different spatial patterns, but as any spatial/textural measures, lacunarity is highly scale dependent (Myint and Lam, 2004).

Lacunarity – Gray-scale Approach

Lacunarity is not confined to binary configurations, but can also be used with gray-scale data (Plotnick, *et al.*, 1996). Remotely sensed image data generally has three-dimensional structure (i.e., x coordinate, y coordinate, z value). As discussed earlier, continuous image data can be transformed into four or more binary images by using the formula and threshold value to obtain lacunarity values. However, the binary images derived from one continuous image data are not true representative sets of the original image texture. Some valuable information on the spatial arrangements of objects or heterogeneity of complex texture features may be lost in the process of converting gray-scale images to binary images. Therefore, it was anticipated that lacunarity index value derived from original gray-scale images could provide better accuracy in texture-based image classification.

Voss (1985) proposed a probability approach to estimate the fractal dimension and lacunarity of image intensity surface. The spatial arrangement of the points determines $P(m,L)$. $P(m,L)$ is the probability that there are m intensity points within a box size of L centered about an arbitrary point in an image. Intensity points are referred to as the number points filled in a cube box. Hence, we have

$$\sum_{m=1}^{N} P(m,L) = 1 \qquad (8)$$

where N is the number of possible points in the box of L. Suppose that the total number of points in the image is M. If one overlays the image with boxes of side L, then the number of boxes with m points inside the box is (M/m) $P(m,L)$. Hence

$$M(L) = \sum_{m=1}^{N} mP(m,L), \text{ and} \qquad (9)$$

$$M^2(L) = \sum_{m=1}^{N} m^2 P(m,L). \qquad (10)$$

Lacunarity can be computed from the same probability distribution $P(m,L)$. Hence, lacunarity $\Lambda(L)$ is defined as

$$\Lambda(L) = \frac{M^2(L) - (M(L))^2}{(M(L))^2}. \qquad (11)$$

A worked example for computing a lacunarity value is documented in Myint and Lam (2004). In applying lacunarity analysis, both the gliding box size and the size of moving window play an important role. Myint and Lam (2004) found that a cube size of 3 × 3 × 3 was the most accurate, and hence this box size was used to compute the lacunarity values in the gray-scale analysis.

Fractal (Triangular Prism Method)

Myint (2003a) examined and evaluated a number of fractal techniques: the isarithm method (Lam and De Cola, 1993), the variogram (Mark and Aronson, 1984), and the triangular prism methods (Clarke, 1986) using a software package known as the Image Characterization and Modeling System (ICAMS) (Quattrochi *et al.*, 1997; Lam *et al.*, 1998). The evaluation was based on a discriminant analysis of texture samples generated from Advanced Thermal Land

Application Sensor (ATLAS) image data. The study reported that the triangular prism was the most accurate method among all three fractal approaches in discriminating different textures of land-use and land-cover categories (Myint, 2003a). Hence, for comparison purposes, the fractal triangular prism approach to extract texture features of urban categories was employed.

This method calculates the surface areas defined by triangular prisms. To use the triangular prism method, a remote sensing image is considered as being located on a grid of x and y coordinates. At each coordinate pair, the value of the pixel is interpreted as the z value; Figure 2 illustrates this arrangement in detail. If an entire image is filled with the same digital value, the results of the structure will be a cube, and this would give a fractal dimension of 2.0. If an entire image is filled with highly uncorrelated values and forms a complex structure, the fractal dimension would be close to 3.0. The points A, B, C, D in Figure 2 are the coordinates of the four pixels on a square grid. The height of O is the average of the elevations from the corner pixels so that: O = (AE + BF + CG + DH)/4. The vertex of this line is connected to the vertex of each of the four corners. This will result in a triangular prism structure. The four prism surfaces that result are OEF, OFG, OGH, and OHE. The areas of these surfaces can be computed using trigonometric formulae. The area of the triangular prism is summed starting from the top left corner of the image. Hence, the area of surfaces for different step sizes can be obtained. The logarithm of the total surface area is plotted against the logarithm of the square of the varying step sizes. The fractal dimension is computed by performing a regression on this pair of variables, and D = 2.0 (slope of the regression line). The dimension value is obtained within a particular window and assigned to the center pixel as the window moves throughout the entire image.

Spatial Autocorrelation (Moran's *I*)

Moran's *I* is one of the two indices of spatial autocorrelation which could describe the degree to which objects in space are similar or which could represent the spatial complexity or the neighborhood arrangements of the surface structures. Moran's *I* is defined as:

$$I(x) = \frac{n \sum_{i}^{n} \sum_{j}^{n} w_{ij} z_i z_j}{W \sum_{i}^{n} z_i^2} \qquad (12)$$
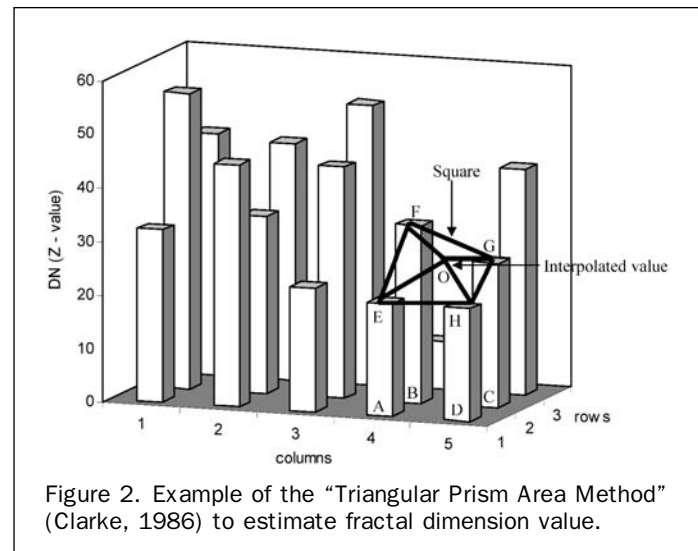
Figure 2. Example of the "Triangular Prism Area Method" (Clarke, 1986) to estimate fractal dimension value.

where w_{ij} is the weight at distance d so that $w_{ij} = 1$ if point j is within distance x from point i; otherwise, $w_{ij} = 0$; z's are deviations (i.e., $z_i = y_i - y_{mean}$ for variable y), and W is the sum of all the weights where $i \neq j$. Moran's I varies from +1.0 for perfect positive correlation (a clumped or smooth pattern) to -1.0 for perfect negative correlation (checker-board pattern).

Analysis

Analysis Using Sample Images

As an initial step towards understanding the effectiveness of different spatial techniques, linear discriminant analysis was employed to identify the same seven urban land-use and land-cover categories: agriculture, commercial, woodland, residential-1, water, residential-2, and grassland. We generated ten samples (33 × 33) for each of the above categories from the Ikonos image data using band 3. Lacunarity, fractal, spatial autocorrelation, and mean value for each sample were later computed. The 33 × 33 sample size was selected due to the nature of the fractal approach. It was discussed earlier that self-similarity of features, shapes, areas, and distances need to be observed at different scales (2^N), and a regression analysis between them needs to be performed to estimate the fractal dimension value. For example, we can obtain only a few steps or observations (e.g., $2^5 = 32$) from a 33 × 33 window size to perform a regression analysis for its fractal estimate.

Sample images of the seven categories are shown in Figure 3. Mean and standard deviation of the image samples were plotted to demonstrate the spatial complexity and nature of the selected classes (Figure 4 and Table 1). It is not surprising that standard deviations of commercial, residential-1, and residential-2 class samples are very high compared to other classes. Moreover, standard deviations of commercial samples are not only very high, but also fluctuate greatly (Figure 4). By observing Figure 4, it can be expected that high values of standard deviation in residential and commercial classes will produce errors when using original spectral bands with conventional spectral-based classifiers. Water is the most homogeneous of all selected classes, and standard deviations of agriculture, grassland, and woodland samples appeared in between the above classes.

For lacunarity calculation, we employed 3 × 3 × 3 cube sizes since the previous study (Myint and Lam, 2004) found that this cube size provided the highest accuracy. The computed values generated by lacunarity, fractal, spatial
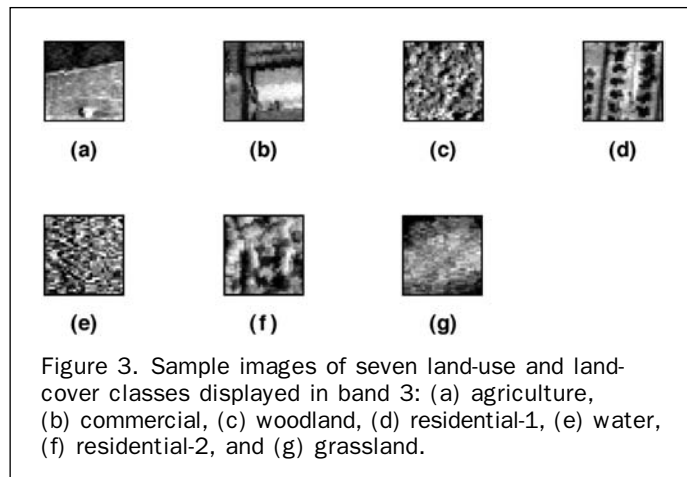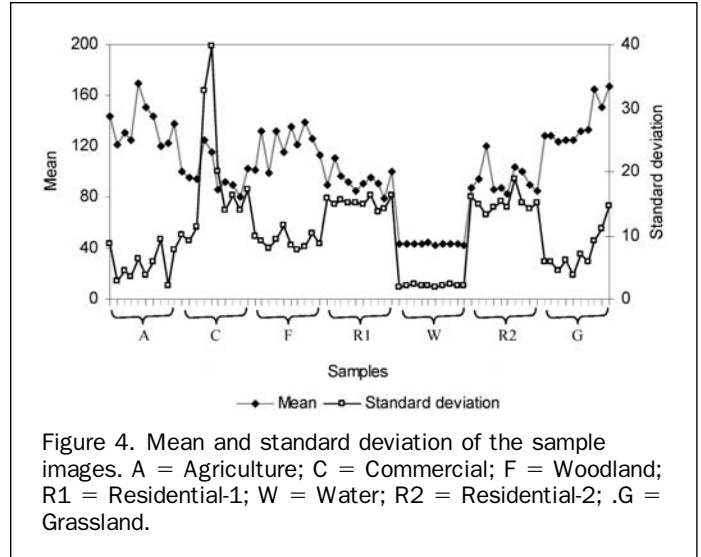
Figure 4. Mean and standard deviation of the sample images. A = Agriculture; C = Commercial; F = Woodland; R1 = Residential-1; W = Water; R2 = Residential-2; .G = Grassland.

autocorrelation, and mean value of the original data were subject to discriminant analysis. The procedure generates a discriminat function (or, for more than two groups, a set of discriminant functions) based on linear combinations of the predictor variables, which provides the best discrimination between the groups. Since lacunarity indices were relatively low, the original values were multiplied by 10 for better observation and comparison purposes. However, the discriminant power of lacunarity approach will be the same. Table 1 lists all the indices generated by different approaches in comparison with the original image sample values. The power of the above approaches in discriminating samples of the selected classes are shown in Table 2. The overall classification accuracy of mean of the original DN values, fractal, spatial autocorrelation, and lacunarity gray-scale approach are 40 percent, 41 percent, 46 percent, and 56 percent, respectively, which clearly shows that the lacunarity approach is the most accurate and the mean of the original DN value approach is the least accurate.

Analysis With Whole Images

The computed values of all approaches (i.e., lacunarity – gray scale, lacunarity – binary, fractal – triangular prism, and spatial autocorrelation – Moran's I) were assigned to the center pixel of the local moving window ($W \times W$), and the window moves throughout the whole image. In the previous study, lacunarity gray-scale method using different moving windows (i.e., 13 × 13, 21 × 21, 29 × 29) were employed to observe the nature and effectiveness of moving windows in characterizing urban texture features. It was reported in an earlier study that a 29 × 29 window size gave the highest accuracy (Myint and Lam, 2004). Hence, we used 29 × 29 window size to evaluate the effectiveness of lacunarity in comparison with fractal, spatial autocorrelation, and original spectral bands in this study. Similarly, the gliding box of 3 × 3 (for the binary approach) and a 3 × 3 × 3 cube (for the gray-scale approach) were found to be more accurate than larger box sizes and cube sizes in discriminating land-use land-cover features. Hence, a 3 × 3 gliding box size for the binary approach and a 3 × 3 × 3 cube size for the gray-scale approach with the use of a 29 × 29 window size were used to generate texture-transformed images.

We used the combination of multi-spectral bands and their texture-transformed images derived from all selected approaches. To better evaluate and for comparison purposes, the traditional multi-spectral band approach was also

Figure 3. Sample images of seven land-use and land-cover classes displayed in band 3: (a) agriculture, (b) commercial, (c) woodland, (d) residential-1, (e) water, (f) residential-2, and (g) grassland.

TABLE 1. DESCRIPTIVE STATISTICS (I.E., MINIMUM, MAXIMUM, MEAN, AND STANDARD DEVIATION) OF THE COMPUTED VALUES OF IMAGE SAMPLES USING ALL SELECTED APPROACHES

		A	C	F	R1	W	R2	G
Original DN Value	Mean	136.32	97.96	121.34	93.05	43.49	93.49	137.65
	Std. Dev.	15.75	13.61	13.85	8.56	0.82	11.41	16.76
	Minimum	120.16	80.08	98.59	79.28	42.32	82.76	124.02
	Maximum	168.87	124.85	138.72	110.58	45.17	119.70	167.02
Fractal Triangular Prism	Mean	2.74	2.55	2.80	2.72	2.92	2.66	2.76
	Std. Dev.	0.13	0.15	0.06	0.08	0.05	0.05	0.14
	Minimum	2.56	2.30	2.73	2.58	2.87	2.61	2.50
	Maximum	2.90	2.82	2.90	2.80	3.02	2.79	2.93
Spatial Autocorrelation	Mean	0.86	0.85	0.61	0.73	0.39	0.76	0.79
	Std. Dev.	0.06	0.06	0.06	0.01	0.10	0.02	0.10
	Minimum	0.76	0.74	0.52	0.71	0.24	0.72	0.65
	Maximum	0.96	0.95	0.69	0.75	0.54	0.78	0.93
Lacunarity Gray Scale	Mean	0.61	1.04	0.87	1.37	0.75	0.62	1.11
	Std. Dev.	0.06	0.17	0.11	0.07	0.04	0.04	0.36
	Minimum	0.54	0.83	0.71	1.10	0.69	0.56	0.13
	Maximum	0.72	1.26	1.04	1.95	0.81	0.67	1.33

A = Agriculture; C = Commercial; F = Woodland; R1 = Residential-1; W = Water; R2 = Residential-2; .G = Grassland.

TABLE 2. THE EFFECTIVENESS OF THE SELECTED SPATIAL APPROACHES IN DISCRIMINATING SAMPLES OF THE SELECTED CLASSES

	Selected Approaches (33 × 33 windows)							
	Mean (DN value)		Fractal		Spatial AutoC		Lacunarity (grey)	
Class	Producer's Accuracy	User's Accuracy	Producer's Accuracy	User's Accuracy	Producer's Accuracy	User's Accuracy	Producer's Accuracy	User's Accuracy
A	10	17	0	0	30	21	60	50
R1	30	33	60	55	60	40	10	33
R2	40	24	40	33	80	73	60	55
W	60	38	20	40	10	25	70	54
G	100	100	100	56	90	90	100	77
F	10	33	70	44	50	63	50	63
C	30	33	0	0	0	0	40	40
Overall Accuracy		40		41		46		56

A = Agriculture; C = Commercial; F = Woodland; R1 = Residential-1; W = Water.

employed. This was just to determine if the traditional multi-spectral approach could provide a satisfactory accuracy for urban classification. We examined different band combinations in the earlier study (Myint and Lam, 2004) and found that the combination of all texture transformed bands and the original bands gave the highest accuracy. Hence, we used a combination of texture-transformed images of band 4, band 3, and band 2 derived from each approach (i.e., lacunarity gray scale, lacunarity binary, fractal triangular, spatial autocorrelation) and the original bands for classification using a 29 × 29 local moving window. An example of texture-transformed images of Ikonos band 3 using the lacunarity gray-scale, the fractal triangular prism, and spatial autocorrelation approach is shown in Figure 5a, 5b, and 5c.

Approximately 30 × 30 pixels of five training samples for each land-use and land-cover category were used as training samples, and 250 random points were used for classification accuracy assessment. To be consistent with all approaches in urban image analysis and for comparison of classification accuracies, we used the same training samples and employed a maximum likelihood algorithm for all band combinations. All lacunarity, fractal, and spatial autocorrelation approaches for texture analysis and image classification were developed using the C++ programming language.

Results and Discussion
It was found that traditional multispectral classification (i.e., band 4, band 3, band 2) was inaccurate for urban image classification from high-resolution data, since it produced 55 percent overall accuracy (Table 3a). This is because spectral-based classification approaches consider individual pixel value and ignore spatial arrangements of neighborhood pixels. For example, roads, houses, grasses, trees, bare soil, shrubs, swimming pools, driveways, and sidewalks, each of which may have a completely different spectral response, but may need to be considered together as a residential class. Hence, to identify urban land-use and land-cover classes, we need to consider the spatial arrangements of neighborhood features and objects or texture and pattern, in addition to considering individual pixel values (Myint et al., 2002). Although producer's accuracies for grassland and woodland were 100 percent, their user's accuracies were found to be the lowest (i.e., 20 percent, 43 percent) among all classes. This means that the number of correctly classified pixels of grassland and woodland classes and the total number of reference pixels for these classes were same. In other words, no pixel from other classes was mistakenly identified as grassland or woodland. However, the ratio of the number of correctly classified pixels of theses classes to the total number of samples being classified as these classes was high. There were many pixels
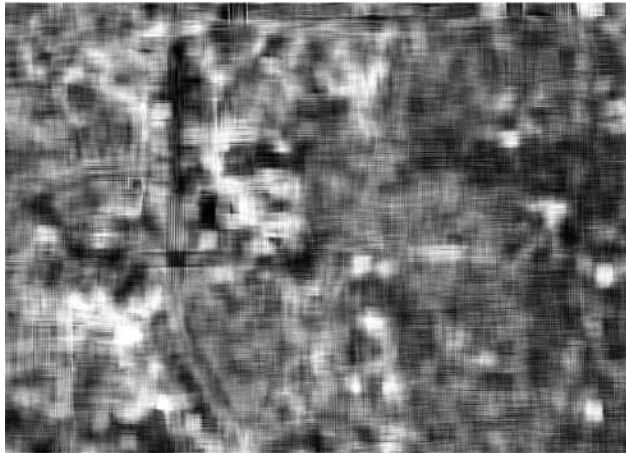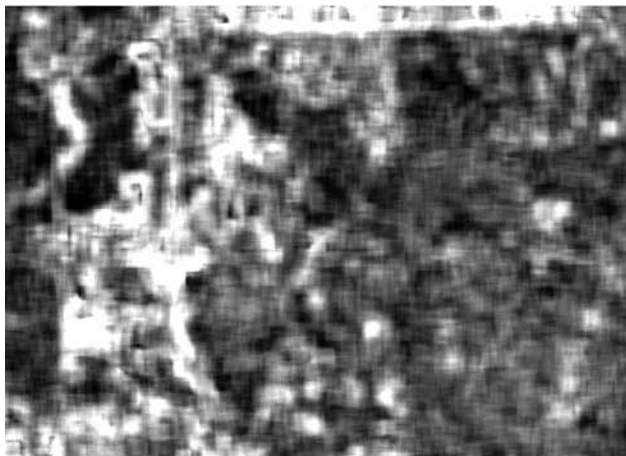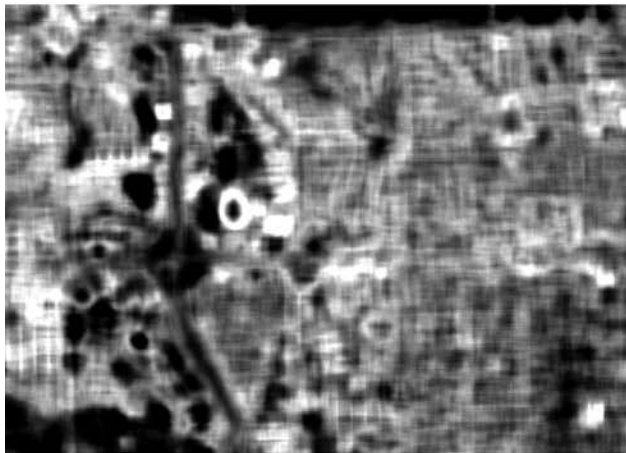
Figure 5. Texture transformed images of Ikonos band 3:
(a) the fractal triangular prism band, (b) spatial autocorrelation band, (c) lacunarity gray-scale band.

identified as these classes in the output map that actually belonged to other classes. The reason was that there were some signature confusions between a number of classes:

agriculture versus grassland and residential-2 versus woodland. This is not a surprising result, as we anticipated and discussed earlier, the similarity of their spatial appearances. These findings show the weakness of original spectral band approach in discriminating different urban land-use and land-cover classes. The classes that produced a lower level of user's and producer's accuracies were commercial, agriculture, and residential-1 classes.

From Table 3b, we can conclude that the fractal (triangular prism) approach was the least accurate (52 percent overall accuracy) approach of all. The fractal approach yields a lower accuracy of the original multi-spectral band approach (55 percent overall accuracy). By observing the output texture-transformed image of the fractal approach in Figure 5a, we can expect that the fractal approach would not provide acceptable classification accuracy. This may be because the remotely sensed images of the land-cover units may not be true fractals, and many natural objects are fractal only in a limited scale range. Consequently, fractal dimensions obtained for the samples of the same feature class may vary significantly. Moreover, completely different texture features may also share the same fractal dimension value (Myint, 2003a). This is due to the fact that fractal dimensions may be far from providing a complete characterization of a set's texture (Mendelbrot, 1995).

For the original spectral band approach, producer's accuracies for grassland and woodland were the highest (92 percent and 75 percent); however, user's accuracies for these classes were found to be the lowest (31 percent and 10 percent). We can say that only 10 percent of the pixels identified as woodland class and 31 percent of grassland class were actually identified as such classes. The user's accuracy represents the probability that a pixel classified into a given category actually represents that category on the ground. That is, even though 92 percent and 75 percent of the grassland and woodland areas were correctly identified as grassland and woodland respectively, only 31 percent and 10 percent of the areas identified as grassland and woodland within the classification are truly these categories. The situations for commercial, agriculture, and residential-1 classes were similar to original spectral band approach. Their producer's and user's accuracies were found to be relatively low.

Spatial autocorrelation (Moran's I) was found to be more accurate (78 percent) than the fractal approach (Table 3c). User's accuracies for agriculture and grassland were 54 percent and 73 percent, whereas producer's accuracies were 100 percent and 27 percent, respectively. Apparently, there is some serious signature confusion between these classes with the spatial autocorrelation approach. It was found that 20 sample points from the agriculture class in the output map actually belonged to the grassland category, and only eight points were accurately identified as such. We can say that the identification of other classes with this approach was reasonably accurate. However, spatial autocorrelation is not powerful enough in distinguishing grassland from agriculture since they both are homogeneous features. We can interpret that spatial autocorrelation approach may be effective in discriminating smooth and coarse surfaces but may not be sensitive to the degree of smoothness or the degree of coarseness. Lee and Wong (2000) and Getis and Ord (1992) reported that spatial autocorrelation is incapable of differentiating hot spots and cold spots.

From Table 3d, the second highest classification accuracy was produced by the lacunarity-binary approach with an overall accuracy of 81 percent, which is below the minimum mapping accuracy of the 85 percent required for most resource management applications (Townshend, 1981). This may be due to the fact that much texture information might have been lost when converting from the original image to four binary images. The most confusing classes for the binary approach are again agriculture and grassland. It

| | Selected Approaches | | | | | | | | | | | | | | |
| | Original Bands | | | Fractal | | | Spatial Autoc | | | Lacu (binary) | | | Lacu (grey) | | |
Class	Pro Acc	Usr Acc	Kap	Pro Acc	Usr Acc	Kap	Pro Acc	Usr Acc	Kap	Pro Acc	Usr Acc	Kap	Pro Acc	Usr Acc	Kap
A	48	53	0.44	47	50	0.40	54	100	1.00	63	100	1.00	77	100	1.00
R1	43	57	0.46	34	77	0.65	71	90	0.88	73	73	0.69	89	89	0.85
R2	37	83	0.75	45	73	0.65	93	87	0.85	78	97	0.96	94	94	0.92
W	100	85	0.84	100	100	1.00	100	100	1.00	100	100	1.00	100	100	1.00
G	100	20	0.18	92	31	0.27	73	27	0.22	100	43	0.39	95	75	0.72
F	100	43	0.39	75	10	0.08	100	67	0.63	100	83	0.81	94	100	1.00
C	70	53	0.47	70	47	0.41	93	83	0.81	85	77	0.73	98	95	0.94
Ovr Kap			0.47			0.41			0.74			0.78			0.90
Ovr Acc		55			52			78			81			92	

A = Agriculture; R1 = Residential-1; R2 = Residential-2; W = Water; G = grassland; F = Woodland; C = Commercial; Pro Acc = Producer's Accuracy; Usr Acc = User's Accuracy; Ovr Acc = Overall Accuracy; Kap = Kappa statistics; Autoc = Autocorrelation; Lacu = Lacunarity.

was found that 13 sample points identified as grassland actually belonged to agriculture, and only 13 points were correctly identified as such. Other signature confusions found were that six sample points from commercial areas actually belonged to residential-1 and four sample points from residential-1 actually belonged to residential-2. This is simply because these categories are the most heterogeneous among all classes that generally possess high variance values.

Table 3e shows that combination of the original spectral bands and the texture transformed of lacunarity gray scale approach was the best approach, since it achieved the highest accuracy (92 percent). Classes with some signature confusion were residential-1 versus residential-2 and agriculture versus grassland. It was found that three sample points identified as grassland actually belonged to agriculture, two sample points identified as residential-1 actually belonged to residential-2, and three samples identified as grassland actually belonged to residential-1.

In examining the accuracy of all approaches, it can be observed that there was always some signature confusion between agriculture and grassland, because they are both spectrally and spatially similar to each other. In general, they were the two major categories that made the classification accuracy lower. Moreover, there is also some major confusion between residential-1 and residential-2, since they both are similar. The other class that had some confusion with others in almost all approaches was commercial class, which has high variance values as residential classes (Figure 4). The only highly reliable category found was water in this study. It reaches the highest user's and producer's accuracy (100 percent) for almost all approaches.

The output maps from the traditional multispectral approach, fractal, spatial autocorrelation, and lacunarity gray scale approaches are shown in Figure 6, 7, 8, and 9, respectively. As mentioned earlier, we used the same training samples, the same number of random points for accuracy assessment, and the same classification algorithm for all approaches. We also applied the same color scheme to each category in the output maps: yellow for agriculture, cyan for commercial, green for woodland, black for water, purple for residential-1, and red for residential-2.

Conclusions

The overall accuracies in this study for fractal, conventional spectral approach, spatial autocorrelation, lacunarity binary,
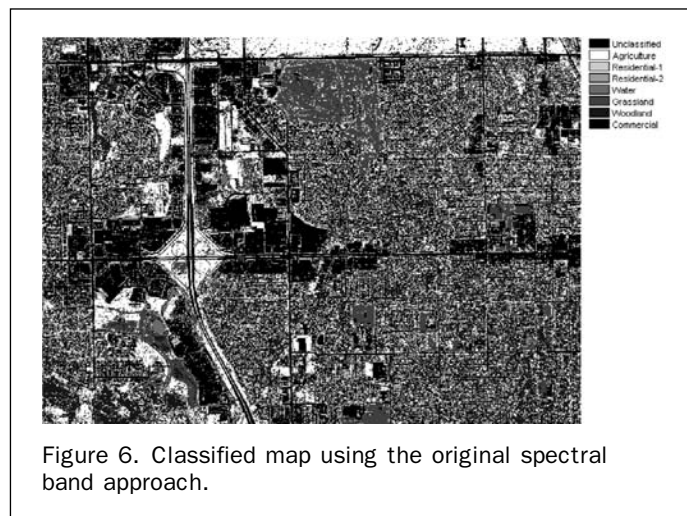
Figure 6. Classified map using the original spectral band approach.
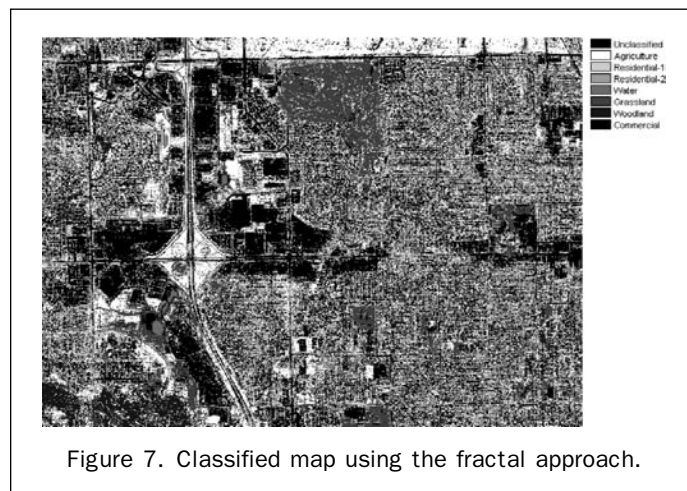
Figure 7. Classified map using the fractal approach.

and lacunarity gray-scale approach were 52 percent, 55 percent, 78 percent, 81 percent, and 92 percent, respectively. The results from the classification of actual image data are consistent with the results from the preliminary study of
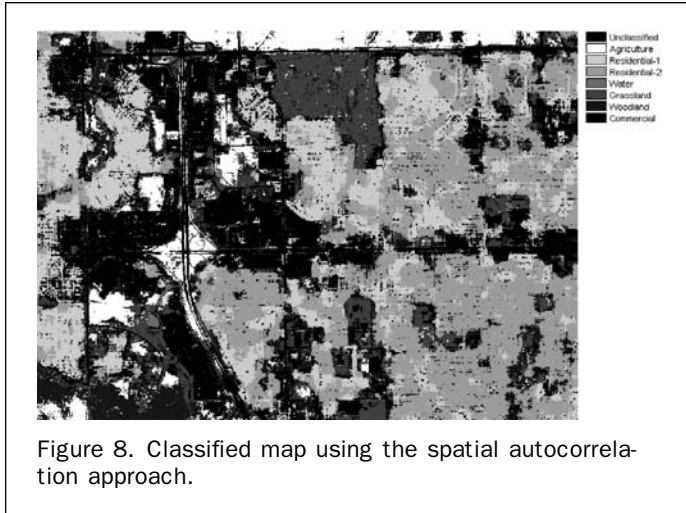
Figure 8. Classified map using the spatial autocorrelation approach.
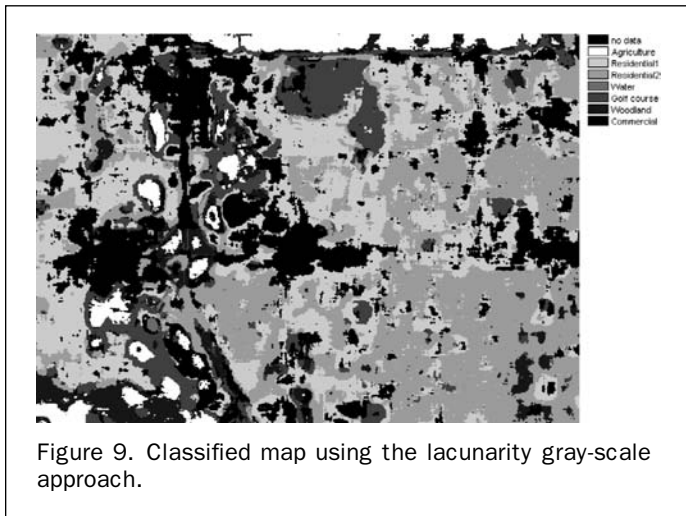
Figure 9. Classified map using the lacunarity gray-scale approach.

sample images using discriminant analysis (Table 2). It has been confirmed by the results obtained in this study that traditional spectral based classification approach is inaccurate in classifying urban land categories from high-resolution image data. Combining the original multi-spectral bands and texture transformed images derived from the fractal approach gave lower accuracy than spectral bands alone. Hence, it can be concluded that the fractal approach is not efficient in land cover classification in high-resolution remotely sensed images. The spatial autocorrelation approach yielded higher accuracy than the fractal approach in urban feature classification.

Lacunarity was found to be the most accurate, and the addition of a lacunarity-transformed image improves the classification accuracy dramatically. Future study should focus on experimenting with different window sizes and gliding box sizes for higher detailed land use land cover classification. Other lacunarity approaches which may better describe the spatial arrangements of urban land-use and land-cover classes could also be explored for future research.

Acknowledgments

References

Allain, C., and M. Cloitre, 1991. Characterizing the lacunarity of random and deterministic fractal sets, *Physics Review, A*, 44:3552–3558.

Anderson, J.R., E.T. Hardy, J.T. Roach, and R.E. Witmer, 1976. *A Land Use and Land Cover Classification System for Use with Remote Sensor Data*, U.S. Geological Survey Professional Paper, 964.

Arai, K., 1993. A classification method with a spatial-spectral variability, *International Journal of Remote Sensing*, 14: 699–709.

Barnsley, M.J., S.L. Barr, and G.J. Sadler, 1991. Spatial re-classification of remotely sensed images for urban land-use monitoring, *Proceedings of Spatial Data 2000*, Oxford, 17–20 September, Remote Sensing Society, Nottingham, pp. 106–117.

Bian, L., and Walsh, S.J., 1993. Scale dependencies of vegetation and topography in a mountainous environment of Montana, *Professional Geographer*, 45(1):1–11.

Brown, D.G., 1998. Classification and boundary vagueness in mapping presettlement forest types, *International Journal of Remote Sensing*, 12(2):105–129.

Burrough, P.A. (1993). Soil variability: A late 20th century view, *Soils and Fertilizers*, pp. 529–562.

Clarke, K.C., 1986. Computation of the fractal dimension of topographic surfaces using the triangular prism surface area method, *Computers and Geosciences*, 12(5):713–722.

Crews-Meyer, K.A., 2002. Characterizing landscape dynamism using paneled-pattern metrics, *Photogrammetric Engineering & Remote Sensing*, 68(10):1031–1040.

De Jong, S.M., and P.A. Burrough, 1995. A fractal approach to the classification of Mediterranean vegetation types in remotely sensed images, *Photogrammetric Engineering & Remote Sensing*, 61:1041–1053.

Dong, P., 2000. Lacunarity for spatial heterogeneity measurement in GIS, *Geographic Infromation Sciences*, 6(1):20–26.

Edwards, G., R. Landary, and K.P.B. Thomson, 1988. Texture analysis of forest regeneration sites in high-resolution SAR imagery, *Proceedings of the International Geosciences and Remote Sensing Symposium* (IGARSS '88), ESA SP-284 (Paris: European Space Agency), pp. 1355–1360.

Emerson, C.W., N.S.N. Lam, and D.A. Quattrochi, 1999. Multi-scale fractal analysis of image texture and pattern, *Photogrammetric Engineering & Remote Sensing*, 65(1):51–61.

Ferro, C.J.S., and T.A. Warner, 2002. Scale and texture in digital image classification, *Photogrammetric Engineering & Remote Sensing*, 68(1):51–63.

Florida Bureau of Comprehensive Planning, 1976. *The Florida Land Use and Land Cover Classification System*, Florida Bureau of Comprehensive Planning Report DSP-BCP-17–76, Tallahassee, Florida.

Foster, B.C., 1985. An examination of some problems and solutions in monitoring urban areas from satellite platforms, *International Journal of Remote Sensing*, 6:139–151.

Franklin, S.E., R.J. Hall, L.M. Moskal, A.J. Maudie, and M.B. Lavigne, 2000. Incorporating texture into classification of forest species composition from airborne multispectral images, *International Journal of Remote Sensing*, 21(1):61–79.

Gallo, K.P., A.L. McNab, T.R. Karl, J.F. Brown, J.J. Hood, and J.D. Tarpley, 1993. The use of a vegetation index for assessment of the urban heat island effect, *International Journal of Remote Sensing*, 14(11):2223–2230.

Gefen, Y., Y. Meir, and A. Aharony, 1983. Geometric implementation of hypercubic lattices with noninteger dimensionality by use of low lacunarity fractal lattices, *Physical Review Letters*, 50:145–148.

Getis, A., and Ord, J.K., 1992. The analysis of spatial association by use of distance statistics, *Geographical Analysis*, 24(3):189–207.

Gong, P., and P.J. Howarth, 1990. The use of structural information for improving land cover classification accuracies at the rural urban fringe, *Photogrammetric Engineering & Remote Sensing*, 56(1):67–73.

Green D.R., R. Cummins, R. Wright, and J. Miles, 1993. A methodology for acquiring information on vegetation succession from remotely sensed imagery, *Landscape Ecology and Geographic Information Systems* (R. Haines-Young, D.R. Green, and S. Cousins, editors), Taylor and Francis, London, pp. 111–128.

Gustafson E.J., 1998. Quantifying landscape spatial pattern: what is the state of the art?, *Ecosystems* 1:143–156.

Haines-Young, R., and M. Chopping, 1996. Quantifying landscape structure: a review of landscape indices and their application to forested landscapes, *Progress in Physical Geography* 20: 418–445.

Haralick, R.M., K. Shanmugan, and J. Dinstein, 1973. Textural features for image clasification, *IEEE Transactions on Systems, Man, and Cybernetics*, SMC-3(6), 610–621.

Huang, Y.J., H. Akbari, H. Taha, and A.H. Rosenfeld, 1987. The potential of vegetation in reducing summer cooling loads in residential buildings, *Journal of Climate and Applied Meteorology*, *2*6:1103–1116.

Jaggi, S., D.A. Quattrochi, and N.S.N. Lam, 1993. Implementation and operation of three fractal measurement algorithms for analysis of remote-sensing data, *Computer and Geosciences*, 19(6):745–767.

Jensen, J.R., and D.C. Cowen, 1999. Remote sensing of urban/suburban infrastructure and socio-economic attributes, *Photogrammetric Engineering & Remote Sensing*, 65(5):611–622.

Journet, D., 1999. Quartiles: How to calculate them?, *http://www.haiweb.org/medicineprices/manual/quartiles_iTSS.pdf*, (last date accessed: 28 April 2005).

Kaplan, L.M., 1999. Extended fractal analysis for texture classification and segmentation. *IEEE Transactions on Image Processing*, 8:1527–1585.

Keller, J.M., S. Chen, and R.M. Crownover, 1989. Texture description and segmentation through fractal geometry, *Computer Vision, Graphics, and Image Processing*, 45:150–166.

Kiema, J.B.K., and H.P. Bahr, 2001. Wavelet compression and the automatic classification of urban environments using high resolution multispectral imagery and laser scanning data, *GeoInformatica*, 5(2):165–179.

Klinkenberg, B., and M.F. Goodchild, 1992. The fractal properties of topography: A comparison of methods, *Earth Surface Processes and Landforms*, 17:217–234.

Lam, N.S.N., and D.A. Quattrochi, 1992. On the Issues of scale, resolution, and fractal analysis in the mapping sciences, *Professional Geographer*, 44(1):88–97.

Lam, N.S.N., and L. De Cola, 1993. Fractal Simulation and Interpolation, *Fractals in Geography* (N.S.N. Lam and L. De Cola, editors), Prentice Hall, Englewood Cliffs, New Jersey, pp. 56–74.

Lam, N.S.N., D. Quattrochi, H. Qui, and W. Zhao, 1998. Environmental assessment and monitoring with image characterization and modeling system using multiscale remote sensing data, *Applied Geographic Studies*, 2(2):77–93.

Lee, J., and D.W.S. Wong, 2000. *Statistical Analysis With ArcView GIS*, John Wiley & Sons, Inc., New York, 189 p.

Lin, B., and Z.R. Yang, 1986. A suggested lacunarity expression for Sierpinski carpets, *Journal Physics A: Mathematical and General*, 19:L49-L52.

Lo, C.P., D.A. Quatrochi, and J.C. Luvall, 1997. Application of high-resolution thermal infrared remote sensing and GIS to assess the urban heat island effect, *International Journal of Remote Sensing*, 18(2):287–304.

Mandelbrot, B.B., 1983. *The Fractal Geogetry of Nature*, New York: Freeman and Company.

Mandelbrot, B., 1995. Measures of fractal lacunarity: Minkowski content and alternatives, *Progress in Probability*, 37:15–42.

Mark, D.M., and P.B. Aronson 1984. Scale dependent fractal dimensions of topographic surfaces: an empirical investigation with applications in geomorphology and computer mapping, *Mathematical Geology*, 16:671–683.

Metzger, J.P., and E. Muller, 1996. Characterizing the complexity of landscape boundaries by remote sensing, *Landscape Ecology*, 11:65–77.

Muller E., 1997. Mapping riparian vegetation along rivers: old concepts and new methods, *Aquatic Botany*, 58:411–437.

Myint, S.W., N.S.N. Lam, and J. Tyler, 2002. An evaluation of four different wavelet decomposition procedures for spatial feature discrimination within and around urban areas, *Transactions in GIS*, 6(4):403–429.

Myint, S.W., 2003a. Fractal Approaches in texture analysis and classification of remotely sensed data: Comparisons with spatial autocorrelation techniques and simple descriptive statistics, *International Journal of Remote Sensing*, 24(9):1925–1947.

Myint, S.W., 2003b. The use of wavelets for feature extraction of cities in satellite images, *Remotely Sensed Cities* (Victor Mesev, editor), Taylor and Francis, London, pp. 109–134.

Myint, S.W., N.S.N. Lam, and J. Tyler, 2004. Wavelet for urban spatial feature discrimination: Comparisons with fractal, spatial Autocorrelation, and spatial Co-occurrence Approaches, *Photogrammetric Engineering & Remote Sensing*, 70(7):803–812.

Myint, S.W., and N.S.N. Lam, 2004. A Study of Lacunarity-Based Texture Analysis Approaches to Improve Urban Image Classification, *Computers, Environment and Urban Systems* (accepted).

Oke, T.R., 1982. The energetic basis of the urban heat island, *Quarterly Journal of the Royal Meteorological Society*, 108:1–24.

Owen, T.W., T.N. Carlson, and R.R. Gillies, 1998. An assessment of satellite remotely sensed landcover parameters in quantitatively describing the climate effect of urbanization, *International Journal of Remote Sensing*, 19:1663–1681.

Pesaresi, M., 2000. Texture analysis for urban pattern recognition using fine-resolution panchromatic satellite imagery, *Geographical and Environmental Modelling*, 4(1):43–63.

Plotnick, R.E., R.H. Gardner, and R.V. O'Neill, 1993. Lacunarity indices as measures of landscape texture, *Landscape Ecology*, 8:201–211.

Plotnick, R.E., R.H. Gardner, W.W. Hargrove, K. Prestegaard, and M. Perlmutter, 1996. Lacunarity analysis: a general technique for the analysis of spatial patterns, *Physical Review* E 53:5461–5468.

Quattrochi, D.A., N.S.N. Lam, H. Qiu, and W. Zhao, 1997. Image Characterization and Modeling System (ICAMS): A geographic information system for the characterization and modeling of multiscale remote sensing data, *Scale in Remote Sensing and GIS* (D.A. Quattrochi and M.F. Goodchild, editors), CRC Press, Boca Raton, Florida, pp. 295–308.

Qiu, H., N.S.N. Lam, D.A. Quattrochi, and J.A. Gamon, 1999. Fractal characterization of hyperspectral imagery, *Photogrammetric Engineering & Remote Sensing*, 65(1):63–71.

Roach, D., and K.B. Fung, 1994. Fractal-based textural descriptors for remotely sensed forestry data, *Canadian Journal of Remote Sensing*, 20:59–70.

Sabins, F.F., 1997. *Remote Sensing Principles and Interpretation*, W.H. Freeman and Company, New York, 494 p.

Sadler, G.J., M.J. Barnsley, and S.L. Barr, 1991. Information extraction from remotely-sensed images for urban land analysis, *Proceedings of the Second European Conference on Geographical Information Systems (EGIS'91)*, Brussels, Belgium, April, EGIS Foundation, Utrecht, pp. 955–964.

Townshend, J.R.G., 1981. *Terrain Analysis and Remote Sensing*, George Allen and Unwin: London, 272 p.

Turcotte, D., 1997. *Fractals and Chaos in Geology and Geophysics*, 2nd Edition, Cambridge University Press, 412 p.

Voss, R., 1986. Random Fractals: characterization and measurement, *Scaling Phenomena in Disordered Systems* (R. Pynn and A. Skjeltorp, editors.), Plenum, New York.

Walsh, S.J., A. Moody, T.R. Allen, and D.G. Brown, 1997. Scale dependence of NDVI and its relationship to mountainous terrain, *Scaling in Remote Sensing and GIS* (Quattrochi, D.A. and M.F. Goodchild, editors), Lewis Publishers, Boca Raton, Florida, pp. 27–55.

Walsh, S.J., L. Bian, S. McKnight, D.G. Brown, and E.S. Hammer, 2003. Solifluction steps and risers, Lee Ridge, Glacier National

Park, Montana, USA: a scale and pattern analysis, *Geomorphology*, 55(1–4):381–398.

Wagrowski, D.M., and R.A. Hites, 1997. Polycyclic aromatic hydrocarbon accumulation in urban, suburban and rural vegetation, *Environmental Science & Technology*, 31(1):279–282.

Woodcock, C.E., A.H. Strahler, and D.L.B. Jupp, 1988. The use of variograms in remote sensing: I. scene models and simulated images, *Remote Sensing of Environment*, 25:323–348.

Wulder, M. and B. Boots, 1998. Local spatial autocorrelation characteristics of remotely sensed imagery assessed with the Getis statistics, *International Journal of Remote Sensing*, 19(11):2223–2231.